Available online at www.sciencedirect.com
SCIENCE DIRECT®
Journal of Solid State Chemistry 177 (2004) 3545–3552
JOURNAL OF SOLID STATE CHEMISTRY
http://elsevier.com/locate/jssc

Metallic behavior of the Zintl phase $EuGe_2$: combined structural studies, property measurements, and electronic structure calculations

Svilen Bobev,[a,*] Eric D. Bauer,[a] Joe D. Thompson,[a] John L. Sarrao,[a] Gordon J. Miller,[b] Bernhard Eck,[c] and Richard Dronskowski[c]

[a] *Los Alamos National Laboratory, Los Alamos, NM 87545, USA*
[b] *Department of Chemistry, Iowa State University, Ames, IA 50011, USA*
[c] *Institut für Anorganische Chemie, Rheinisch-Westfälische Technische Hochschule, 52056 Aachen, Germany*

Received 5 November 2003; received in revised form 4 June 2004; accepted 5 June 2004

Available online 11 August 2004

Abstract

The Zintl compound $EuGe_2$ crystallizes in the trigonal space group $P\bar{3}m1$ (No. 164) with the $CeCd_2$-structure type. Its structure can be formally derived from the hexagonal AlB_2-structure type by a strong puckering of the hexagonal layers. The chemical bonding in $EuGe_2$ can be rationalized according to the Zintl concept as $(Eu^{2+})(Ge^{1-})_2$, since the europium atoms are divalent and each germanium atom receives one additional valence electron. In that sense, $EuGe_2$ is expected to be a closed-shell compound with semiconducting behavior. However, temperature dependent resistivity measurements show $EuGe_2$ to be metallic. Subsequently, detailed crystallographic studies revealed the structure and the composition of $EuGe_2$ to be free of defects and impurities, which, along with the confirmed divalent oxidation state of the europium atoms by means of magnetic measurements, make $EuGe_2$ another example of a metallic Zintl phase. These results are in good agreement with the results of electronic structure calculations such as TB-LMTO-ASA (LDA) and FLAPW (GGA), which reveal non-zero DOS at the Fermi level.

Keywords: Rare-earth intermetallics; Crystal structure; Magnetic measurements; $EuGe_2$; Eu-magnet; Zintl phases; DFT-calculations

1. Introduction

Zintl phases are a special class of intermetallic compounds in which one of the components is far more electropositive than the other(s). Eduard Zintl first studied such binary intermetallic phases and successfully rationalized their structures and properties by proposing electron transfer from the electropositive to the electronegative component rather than an evaluation of the total valence electron concentration (VEC) per atom [1–5]. Thus, Zintl defined a class of compounds that can be considered as intermediate between the typical intermetallic phases on the one hand, and normal valence compounds on the other. In that sense, the fundamental difference between Zintl phases and all other intermetallic phases is the role played by the electronegative components, which accept the electrons from their more electropositive partners to form polyanions. However, if the electropositive component is one of the Lanthanide elements, these intermetallic compounds can display interesting physical properties as well. In particular, many Eu- and Yb-based intermetallic compounds exhibit rather unusual electronic and magnetic properties, such as (1) heavy fermions; (2) spin fluctuations and (3) mixed valency. The majority of these phenomena can be explained if one recognizes that Eu^{2+} and Yb^{2+} are common oxidation states for both elements due to the stabilization of their half-filled and completely filled 4*f*-shells, respectively [6–8].

As part of a broad, systematic effort to study the properties of some ternary Eu- and Yb-based intermetallic compounds as a function of polyanionic network bonding patterns, electron count, electronegativity

*Corresponding author. Current address: 304A Drake Hall, Department of Chemistry and Biochemistry, University of Delaware, Newark, DE 19716, USA.
E-mail address: sbobev@chem.udel.edu (S. Bobev).

0022-4596/$ - see front matter © 2004 Elsevier Inc. All rights reserved.
doi:10.1016/j.jssc.2004.06.018

and size of the constituents, we discovered that the "Zintl phase" $EuGe_2$ showed metallic properties. $EuGe_2$ with divalent Eu^{2+} cations is presumably a closed-shell compound, and would be predicted to have semiconducting behavior. There are, however, relatively few reports of resistivity measurements conducted on Zintl phases, in general, but there are cases in which directed, covalent bonding in the polyanionic network is important, but metallic conduction is evident—such cases are termed "metallic Zintl phases" [2]. On the other hand, the apparent disagreement between metallic character and closed shell chemical bonding has been utilized within the Zintl concept to identify adventitious impurities. For example, semiconducting "Ca_3Pb" [9] was shown to contain oxygen atoms in interstitial sites and is better described as an inverse perovskite, Ca_3PbO [10,11]. Thus, the question arose whether $EuGe_2$ is a "metallic Zintl phase," or achieves its unexpected metallic behavior from adventitious impurities. There are reports that carbon, nitrogen, oxygen [10,11] and even hydrogen [12] are particularly common interstitial atoms in many *AE–Tt* and *RE–Tt* quasi-binary phases (*AE* = alkaline-earth; *RE* = rare-earth; Tt = Tetrel = group 14 element), which provided a strong motivation for undertaking a thorough and systematic study of $EuGe_2$. Herein, we report the reexamined crystal structure (via X-ray powder diffraction), combined with extensive property measurements and first-principles theoretical calculations of the metallic Zintl phase $EuGe_2$.

2. Experimental section

2.1. Synthesis

All starting materials were used as received: Eu (Ames Laboratory, ingot, 99.9% metal basis), Ge (Alfa, pieces, 99.999%). The europium surface was cleaned with a scalpel immediately before use. The stoichiometric $EuGe_2$ mixtures were loaded in alumina crucibles, which were subsequently enclosed in evacuated fused silica jackets by flame-sealing (vacuum ca. 10^{-4} Torr). The reactions were carried out at different temperature profiles, including quick or slow ramping of the temperature up to 1050°C, dwelling at that temperature for up to 72 h and cooling down to room temperature at various rates. No other phases besides some residual elemental Ge (diamond-type) and the trigonal $EuGe_2$ [13] were present according to the powder X-ray diffraction patterns (below). The same or even more $EuGe_2$ deficient reaction outcomes were found when arc-melting pure Eu and Ge in a ratio of 1:2. The probable reason for the loss of Eu during arc-melting reactions or reactions in alumina crucibles is due to its high vapor pressure at temperatures above 822°C. To minimize the loss of elemental Eu during the heating process, reactions in weld sealed Ta-tubes were set up and carried out at similar temperature regime. Under these conditions, the reaction outcome contained considerably less unreacted elemental Ge, but the reaction product was always contaminated with EuGe and $TaGe_2$.

In all instances, the reaction products were inhomogeneous powders and/or polycrystalline pieces. Further arc-melting of the as-cast products and subsequent annealing for prolonged periods of time at ca. 650°C were also explored, but failed to produce quantitative yields and/or good quality single crystals. Therefore, all property measurements discussed herein were carried out on polycrystalline ingots of $EuGe_2$, which appear to be stable in dry air over a period of several weeks.

2.2. X-ray diffraction studies

X-ray powder diffraction patterns were taken on a Scintag XDS 2000 diffractometer with monochromatized Cu$K\alpha$ radiation. The patterns were used both to verify the unit cell parameters by a least-squares refinement of the positions of the lines, calibrated by silicon (NIST) as an internal standard, as well as to refine the structural parameters for $EuGe_2$ by use of the Rietveld method [14]. For that purpose, intensity data were routinely collected in continuous scan mode up to a 2θ limit of 80° with an interval of 0.2°/min. A rotating sample holder made of Ti was utilized for this purpose. Cell parameters, atomic coordinates, isotropic thermal parameters, Eu and Ge site occupancies, background coefficients, scale factor and phase fractions, and peak profile coefficients (both Lorentzian and Gaussian contributions) were refined. The limited number of observed reflections (Table 1) did not allow for the simultaneous refinement of all parameters. Therefore, to assure reasonable data-to-parameter ratio, the atomic coordinates, the thermal parameters, the Eu and Ge site occupancies were refined one at a time. As expected, the refinements confirmed the originally proposed structure and stoichiometry ($P\bar{3}m1$ space group, No. 164), without any partially occupied or disordered sites (Fig. 1). No signs of additional, unaccounted electron density were detected in the difference Fourier map, which suggest $EuGe_2$ has a very narrow homogeneity width and remains free of defects and impurities. This is further corroborated by the virtually constant lattice parameters observed, independent of the method of preparation. It should also be noted that the site occupancies for both Eu and Ge, when refined, did not deviate within more than 4σ from fully occupied. A list of other important crystallographic parameters and details for the refinement are summarized in Table 1; final positional and isotropic thermal parameters and important distances are listed in Table 2.

Table 1
Selected data collection and refinement parameters for $EuGe_2$

Empirical formula	$EuGe_2$
Formula weight	297.18
Space group, Z	$P\bar{3}m1$ (No. 164), 1
Radiation, λ (Å)	Cu$K\alpha$, 1.5406
Temperature (°C)	21(2)
Unit cell parameters	
a (Å)	4.1035(1)
c (Å)	4.9972(3)
V (Å^3)	72.87(4)
ρ_{calcd} (g/cm^3)	6.771
Data/parameter	51/9
R_p/wR_p (%),[a]	2.07/7.39
Reduced χ	2.634

[a] $R_p = \sum||I_{io}|-|I_{ic}||/\sum|I_{io}|$; $wR_p = \{\sum[w_i(I_{io}^2 - I_{ic}^2)^2]/\sum[w_i(I_{io}^2)^2]\}^{1/2}$, where, $w = 1/[\sigma^2 I_{io}^2]$, and I_i is the intensity of the ith observation.

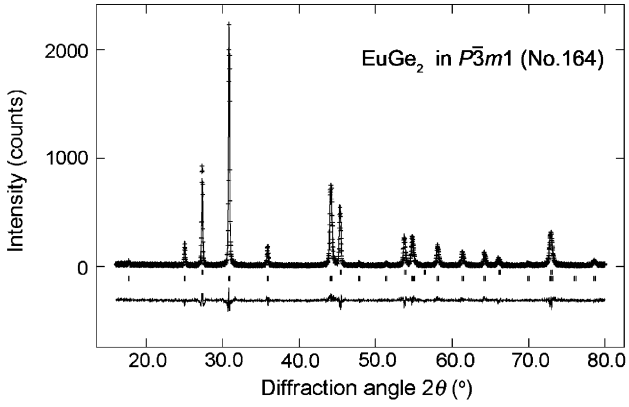

Fig. 1. X-ray powder diffraction pattern of $EuGe_2$, showing the observed (crosses) and the calculated (solid line) intensities. The difference curve is shown below the diffraction pattern and the tic marks: Ge ($Fd\bar{3}m$, top) and of $EuGe_2$ ($P\bar{3}m1$, bottom).

Table 2
Atomic coordinates, isotropic displacement parameters, and important distances (Å) in $EuGe_2$

Atom	Site	x	y	z	SOF[a]	U_{iso} (Å^2)
Eu	1a	0	0	0	1.02(1)	0.015(2)
Ge	2d	1/3	2/3	0.4018(9)	1.07(2)	0.023(2)
Ge–Ge 3×	2.564(4)				Eu–Ge 6×	3.106(3)
Ge–Eu 3×	3.106(3)				Eu–Eu 6×	4.1035(1)

[a] Occupancy factors were refined one at a time, while keeping the remainder of the variables fixed.

2.3. Property measurements

Field cooled magnetization measurements were performed in a Quantum Design MPMS magnetometer from 2 to 350 K in a magnetic field of 0.1 T. The specific heat was measured from 2 to 300 K using a thermal relaxation method. The electrical resistivity measurements were carried out using a four-probe technique from 2 to 300 K with an excitation current of 1 mA. All property measurements were carried out several times on several sample batches to assure reproducibility. Because of the inability to grow single crystals of $EuGe_2$, all measurements were performed on polycrystalline ingots. These were prepared by additional heat-treating the as-cast samples (see Synthesis), and as already mentioned, they inevitably contained some residual germanium. Therefore, the phase fractions for $EuGe_2$ and elemental Ge were elucidated from the corresponding X-ray powder patterns through full profile Rietveld refinement [14].

2.4. Theoretical methodology

Electronic structure calculations of the density-functional type [15–17] on $EuGe_2$ were performed using the tight-binding linear muffin–tin orbital (TB-LMTO) method [18,19] in the atomic-sphere approximation (ASA) and the local spin-density approximation (LDA) [20] and also by means of the full-potential linearized augmented-plane-wave (FLAPW) method [18,21] as implemented in the WIEN2k program package [22] and using the spin-polarized generalized gradient approximation (GGA) according to Perdew et al. [23]. Within the scalar-relativistic LMTO approach, the Eu 4f states were treated as core-like and contained seven unpaired electrons; these were not allowed to covalently interact with the valence region, which consisted of Eu 6s, 5d and Ge 4s, 4p and 4d functions; Eu 6p orbitals were downfolded. For the FLAPW calculations, the Kohn–Sham equations were solved scalar-relativistically for the valence region which was chosen to consist of 4f, 5s, 5p, 5d, 6s orbitals for Eu and of 3d, 4s, 4p orbitals for Ge; energetically lower-lying states were put into the (fully relativistic) core region. Diagonalization and integration of the FLAPW Hamiltonian was eventually performed using a total of 700k points of which 80 were irreducible. At this point, differences in total electronic energies had converged to less than one tenth of a Rydberg, and the spontaneous magnetic moment was stable within 0.1 Bohr magnetons.

3. Discussion

3.1. Structure

REGe$_2$ (RE = Rare-Earth) compounds, or rather REGe$_{2-x}$ ($0 < x < 0.5$), adopt a number of different crystal structure types, largely dependent on the nature of the rare earth element, the stoichiometry, and/or the

reaction conditions. In most cases, the ideal composition is rarely realized and various non-stoichiometric compounds abound. Numerous publications and several reviews report the structures and the properties for many of these germanides, but the number of new phases continues to grow and appears far from being exhausted [24–26].

It is therefore appropriate to give a brief introduction to the most common structure types in which these phases crystallize. The three major types for $RE\mathrm{Ge}_{2-x}$ compounds are: (1) α-ThSi_2 (space group $I4_1/amd$); (2) GdSi_2 (space group *Imma*), and (3) AlB_2 (space group $P6/mmm$), and they are closely related. The structure type depends largely on the nature of the rare earth and is also governed by the degree of non-stoichiometry. For instance, early lanthanides (larger cations) predominantly crystallize in the α-ThSi_2 type, and with decreasing *RE* size, a gradual transition to orthorhombically distorted GdSi_2 type and hexagonal AlB_2 is observed. Additionally, the digermanides with the α-ThSi_2 structure are generally with composition close to the ideal, i.e., $x \sim 0$, while the AlB_2-type is common in higher degrees of non-stoichiometry, i.e., $x \sim 0.25$. The orthorhombic GdSi_2 type occurs in intermediate compositions. In many substoichiometric $RE\mathrm{Ge}_{2-x}$ compounds, partial ordering of the vacancies is possible, which gives rise to novel structure types and superstructures [26].

Despite this wealth of information on rare-earth germanides, the data available for EuGe_2 is very limited. It appears that EuGe_2 is the only rare earth digermanide that crystallizes in the trigonal space group $P\bar{3}m1$, as was recognized from its powder diffraction pattern four decades ago [13]. The binary Eu–Ge phase diagram [27] suggests the existence of seven phases (including the high temperature ones), although only 4 compounds have been structurally characterized so far: (1) $\mathrm{Eu}_2\mathrm{Ge}$ (PbCl_2 structure type) [28]; (2) $\mathrm{Eu}_5\mathrm{Ge}_3$ ($\mathrm{Cr}_5\mathrm{B}_3$ structure type) [29]; (3) EuGe (CrB type) [30], and (4) α-EuGe_2 (low-temperature form, CeCd_2 type) [13]. This makes the Eu–Ge system somewhat unique and definitely provides strong incentive for more thorough and systematic studies.

There are no other rare-earth germanides (or even silicides), which crystallize with that structure [25]. Among more than 100 compounds in that Pearson's family (*hP*3, space group $P\bar{3}m1$, both CdI_2 and CeCd_2 types), the only other chemically related phases are two allotropic forms of BaSi_2 and SrGe_2, respectively [31,32]. This is not surprising because the chemistry of Sr, Ba and divalent Eu is very similar and they often form isostructural compounds. To date, no detailed property measurements and/or theoretical calculations on EuGe_2 have ever been reported beyond a few brief reports on the magnetic properties and ^{151}Eu Mößbauer effect in polycrystalline EuGe_2 [33].

The EuGe_2 structure can be derived from the parent structure type of AlB_2 by a strong puckering of the hexagonal layers (Fig. 2). Through this imaginary process, one half of the germanium atoms in EuGe_2 would be moved above, whereas the other half would be pushed the same distance below the mirror plane, to form arsenic-like layers, separated by the europium atoms (Fig. 2). Further details on the group–subgroup relations in with the archetype are given elsewhere [34]. The Ge–Ge distances are 2.564(4) Å, almost 0.1 Å longer compared with the Ge–Ge contacts in elemental Ge [35]. However, this elongation is not unusual given the fact that each germanium atom is not in tetrahedral coordination and formally carries a charge of "1−". Similar Ge–Ge distances have been observed in other binary Eu–Ge phases and in *RE*–Ge phases in general [24,26,29,30]. In that sense, the chemical bonding in EuGe_2 can be readily rationalized according to the Zintl concept, assuming that the europium atoms are divalent. Hence, each germanium atom from the corrugated layers formally receives one extra electron to become a pseudo-atom of "Ge^{1-}". The latter is thus isoelectronic with arsenic, since both have the same outer electron shell configurations and, indeed, the 2D puckered layers of $[\mathrm{Ge}_2]^{2-}$ are isostructural with elemental gray arsenic (Fig. 2). The divalent europium cations separate these puckered layers and counterbalance the charges.

As mentioned already, the EuGe_2 structure was originally determined from X-ray film methods and, based on that, it was assigned to the CdI_2 type (*hP*3, space group $P\bar{3}m1$, No. 164). However, the *z*-coordinates in EuGe_2 and in CdI_2 type structures are quite different [13,25], ca. 0.4 and 0.25, respectively. So, while the CdI_2 type structure can be easily described as a layered material with nearly van der Waals type interactions between the layers (all other known compounds with the CdI_2 type are halides, sulfides and tellurides, which demonstrate easy [001] cleavage), EuGe_2 exhibits more of a three-dimensional structure due to the much stronger inter-layer bonding. This, in turn, also results in significant Eu–Eu interactions along

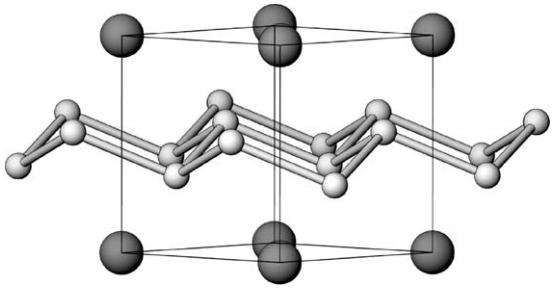

Fig. 2. Schematic representation of the trigonal EuGe_2 structure (projection approximately down the [110] direction). Large, black spheres denote Eu atoms. The small light spheres stand for the Ge atoms.

the c direction, nicely illustrated by the ab initio electronic structure calculations (below). In the midst of this discussion it should also be noted that according to the more recent interpretations [25], the $EuGe_2$ structure is re-assigned to the $CeCd_2$ type. However, the c/a ratio in $CeCd_2$, and the c/a ratio in $EuGe_2$ differ significantly, while the z-coordinates are relatively close [13,25]. This may suggest that the $EuGe_2$, along with the isostructural $BaSi_2$ and $SrGe_2$, should rather be regarded as phases crystallizing in their own structure type.

3.2. Properties

$EuGe_2$ has long been considered as a classic example of a Zintl phase without any other arguments besides the formal electron count, which nicely follows the octet rule [2–5]. ^{151}Eu Mößbauer spectroscopic results confirmed the "2+" oxidation state for the Eu atoms in the structure [33], and thus one should expect $EuGe_2$ to be a closed-shell compound. Therefore, the serendipitous discovery of the metallic behavior of $EuGe_2$ was very surprising and rather unusual. Although there are some known examples in the literature of "metallic" Zintl phases [2–4], this inconsistency between the property measurements and the well-established Zintl concept gave rise to questions concerning the true stoichiometry of $EuGe_2$ with respect to the existence of sub-stoichiometric $EuGe_2$ and/or an impurity stabilized phase. These legitimate concerns became even deeper after recognizing that similar problems have shadowed the chemistry of related AE_5Tt_3 and RE_5Tt_3 compounds with the Cr_5B_3 type structure. Very recently, many erroneous reports of binary AE_5Tt_3 phase were uncovered and the corresponding structures re-determined as AE_5Tt_3X (X=interstitial C, N, O or H), which explained the puzzling properties of these materials [36,37]. Therefore, we carried out thorough and systematic property measurements to fully elucidate the nature of the metallic behavior of the Zintl compound $EuGe_2$.

For this purpose, several batches of $EuGe_2$ were prepared using different synthetic techniques (see Experimental section) and the lattice parameters for each of these were compared with those in the literature. The unit cell volume remained virtually unchanged, which strongly suggested that $EuGe_2$ is indeed a line compound. This is also corroborated by the subsequent Rietveld refinements, which clearly showed no deviations of the site occupancies for both Eu and Ge (Table 2). The final structure refinement converged at low residual values and with well-behaved thermal ellipsoids with no indications for disorder or impurities (to the extent light elements can be detected by means of X-ray diffraction).

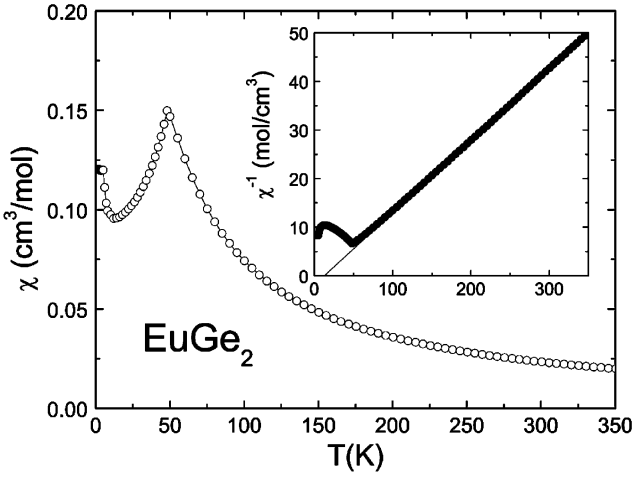

Fig. 3. Magnetic susceptibility $\chi(T)$ of $EuGe_2$ measured in a magnetic field $H = 0.1$ T. Inset: inverse magnetic susceptibility $\chi^{-1}(T)$. The line is a fit of a Curie–Weiss law to the data.

The magnetic susceptibility vs. temperature of $EuGe_2$ is shown in Fig. 3. A cusp-like feature is visible in the data at $\sim$50 K indicating the onset of long-range antiferromagnetic (AFM) order in this material; a Néel temperature $T_N = 48$ K is determined from the midpoint of the jump in $d\chi/dT$. Above the Néel temperature, $\chi(T)$ follow a Curie–Weiss law $\chi(T) = C/(T-\theta_{CW})$, where $C = N_A\mu_{eff}/3k_B$ is the Curie constant as shown in the inset of Fig. 3, yielding an effective moment $\mu_{eff} = 7.34\,\mu_B$, which is significantly lower than that expected for Eu^{2+} ($\mu_{eff} = 7.94\,\mu_B$). It should be noted here that this value was determined from a polycrystalline sample, which contained residual elemental Ge. Although the germanium phase fraction was estimated from the corresponding X-ray powder pattern and the mass of the sample was corrected accordingly, the agreement between the observed and the theoretical moment for Eu^{2+} is not perfect, most likely due to small sample inhomogeneity, which in turn leads to not quite good estimations of the phase fractions obtained from the refined data. The positive Curie–Weiss temperature $\theta_{CW} = +13$ K indicating weak ferromagnetic interactions between the Eu moments, which are well separated from each other; the shortest Eu–Eu contacts are 4.1035(1) Å (Table 2).

However, these interactions are very important in contributing to the metallic properties as demonstrated from the DFT electronic structure calculations (below) although even from the sum of the ionic radii [35,38], one would expect them to be non-bonding. The antiferromagnetic order and an effective moment roughly consistent with divalent Eu indicate a stable divalent electronic configuration of Eu in $EuGe_2$ with little evidence of intermediate valence behavior. This supports the earlier ^{151}Eu Mößbauer spectroscopy

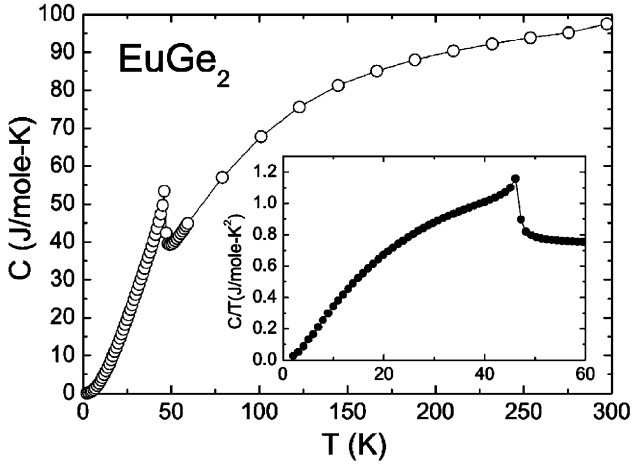

Fig. 4. Specific heat $C(T)$ of $EuGe_2$. Inset: specific heat divided by temperature T of $EuGe_2$ below 60 K.

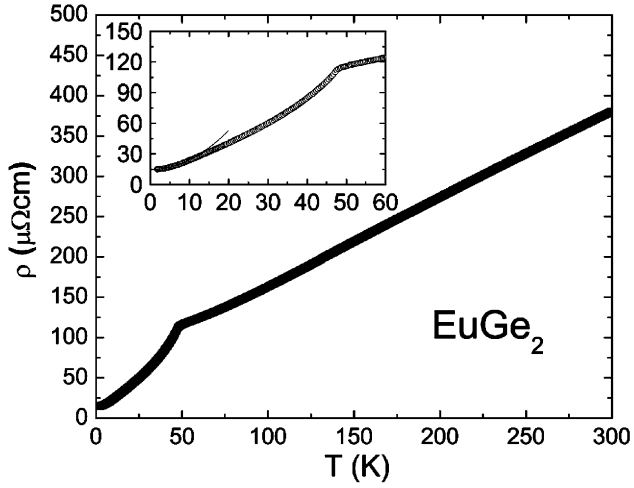

Fig. 5. Electrical resistivity $\rho(T)$ of $EuGe_2$. Inset: $\rho(T)$ below 60 K. At very low temperatures ($\sim$10 K), $\rho(T)$ exhibits a T^2 temperature dependence (shown).

results, which also confirmed the "2+" oxidation state for the Eu atoms in the $EuGe_2$ structure [33].

The specific heat $C(T)$ of $EuGe_2$ is displayed in Fig. 4. An anomaly corresponding to the antiferromagnetic transition is observed at $T_N = 48$ K. The specific heat jump at T_N, $\Delta C|_{TN} \sim 14(5)$ J/mol K, is somewhat smaller than the value predicted by Mean Field Theory (MFT) $\Delta C|_{TN} = 20.1$ J/mol K for $J = S = 7/2$ (Eu^{2+}) [39]. The reason for that might be again error in the determination of the Ge phase fraction in the polycrystalline sample as discussed above (ca. 30–40% by weight according to the Rietveld refinements). An estimate of the magnetic entropy below T_N is obtained by subtracting a Debye contribution [40] to the specific heat with $\theta_D = 260$ K from the data which yields $S_{mag}(48\,K) \sim 18$ J/mol K, consistent with the value ($S_{mag} = R \ln 8 = 17.3$ J/mol K) for $S = 7/2$.

The electrical resistivity $\rho(T)$ of $EuGe_2$ is shown in Fig. 5. A small kink in $\rho(T)$ is found at $T_N \sim 48$ K corresponding to the onset of AFM order as shown in the inset of Fig. 5. In the antiferromagnetic state, the electrical resistivity exhibits a T^2 temperature dependence below $\sim$10 K. A fit of the data to $\rho(T) = \rho_0 + AT^2$ in the range $1.8 < T < 8.3$ K, yields $\rho_0 = 14.7\,\mu\Omega$ cm and $A = 0.10\,\mu\Omega$ cm/K^2. All these observations clearly indicate metallic-like behavior, which is nicely supported by the band-structure calculations (below). Nevertheless, the resistance value is somewhat on the high side for what should be expected from pure metal due almost certainly to grain boundaries and residual elemental germanium.

3.3. Electronic structure calculations

Elemental rare earth metals as well as compounds containing them still represent a major challenge for density-functional theory (DFT) because of their tendency to be strongly correlated materials with highly localized 4*f* electrons. In computational practice, one either treats the 4*f* levels as core levels, thereby often reproducing the correct magnetic ground states but artificially excluding the 4*f* levels from bonding interactions with their surroundings, or alternatively, the 4*f* levels are considered as valence levels, but then the itinerancy of the minority *f* states can be largely overestimated since they appear too close above the Fermi level [41]. The latter DFT artifact is sometimes corrected by introducing an empirical Hubbard *U* parameter [41] for additional intra-atomic electronic repulsion.

For the study of chemical bonding here, the above difficulty in dealing with the 4*f* orbitals as valence levels seems to be less critical, especially if the 4*f* elements build up the cationic entities in chemical compounds. Here, the charge depletion of the rare earth metal's valence regions makes the inner 4*f* electrons more accessible for electronic interactions with their neighborhood. In certain cases, the resulting strong $f-d$ mixing and, likewise, covalent bonding may then even totally quench the formation of localized 4*f* magnetic moments, as exemplified by the (weakly) Pauli paramagnetic cerium nitride, CeN, crystallizing in the rock-salt structure [42].

Fig. 6 displays a theoretical densities-of-states (DOS) curve and crystal orbital Hamilton population (COHP) analysis [43] of $EuGe_2$ on the basis of LMTO theory, excluding the Eu 4*f* levels from the valence wavefunctions. The Fermi level lies in a pseudo-gap-region (DOS at the Fermi level is not zero), and the *weakly* metallic behavior is due to both Ge 4*s*/4*p* and Eu 5*d* contribution; note that the occupied DOS region is almost

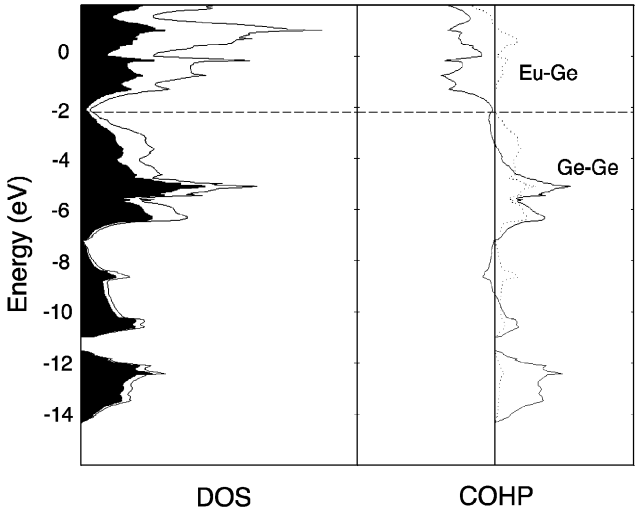

Fig. 6. LMTO DOS and crystal overlap Hamilton population (COHP) curve of $EuGe_2$. The lower lying valence states are primarily Ge 4*s* in character and increase in Ge 4*p* character as states approach the Fermi level. The darkened regions indicate Ge contributions to the total DOS.

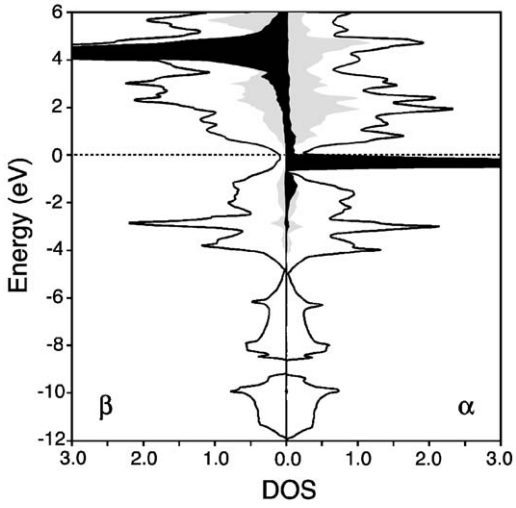

Fig. 7. FLAPW spin-polarized DOS for $EuGe_2$ as a function of the electronic energy; the right and left sides show the DOS for the majority (α) and minority (β) spins, respectively; the Fermi level has been set to the energy zero (dashed line). Eu *d* and *f* contributions to the total DOS have been indicated with gray and black shadings.

entirely Ge-centered. The COHP curves show that both Ge–Ge and Eu–Ge interactions are almost fully optimized up to the Fermi level, with strong Ge–Ge bonding dominating the structure and only a little antibonding in the highest occupied region, due to orbital interactions between adjacent puckered Ge sheets.

Even if the 4*f* levels are included as valence levels, $EuGe_2$ apparently poses no serious problems for a density-functional approach, and the FLAPW-GGA calculation immediately converges to a theoretical saturation moment of $6.97\,\mu_B$ which compares not too badly with the experimental moment of $\sim 7.4\,\mu_B$ (paramagnetic region). The corresponding spin-polarized density-of-states (DOS) of the valence region is given in Fig. 7, clearly characterizing $EuGe_2$ as being a metal. In the occupied, lower part, the DOS is almost completely made up from filled germanium 4*s* and 4*p* contributions, an expected result for the anionic Ge substructure of $EuGe_2$. Note how closely this DOS region resembles—with the exception of the 4*f* states discussed below—the previous DOS (Fig. 6) derived from the simpler LMTO approach. Not surprisingly, spin polarization leaves the Ge orbitals practically untouched since these are magnetically inactive because of insufficient exchange splitting; consequently, the magnetic moment of $EuGe_2$ is localized almost entirely on the europium atom. With the exception of a small contribution just below the Fermi level, europium 5*d* states (in gray) appear mostly in the unoccupied region. The Fermi level, however, cuts through the upper part of the Eu majority 4*f* band (in black, right side) in which the magnetic moment (α-spins) resides. The empty minority 4*f* band (black, left) is 4.7 eV apart, in the virtual region; the latter $\alpha-\beta$ energy difference is probably underestimated by the GGA calculation.

4. Conclusions

To recap, the reported comprehensive and systematic study of the structure, electronic structure and physical properties of the Zintl phase $EuGe_2$ revealed metallic behavior. These properties are due to a non-zero DOS at the Fermi level, which is largely independent from whether or not 4*f* levels are included as valence levels in DFT calculations. If Eu were replaced by a divalent alkaline-earth metal lacking partially filled 4*f* orbitals, such as Sr, this would annihilate the 4*f* states from the Fermi level, and would be expected to be a classical Zintl phase (LMTO-ASA calculations on the high pressure form of $SrGe_2$ show a pseudogap, but non-zero DOS at the Fermi level [44]). The presence of 4*f* states is seen in the results of both FP-LAPW and TB-LMTO calculations when the Eu 4*f* orbitals are considered to be valence orbitals. LMTO calculations in which the 4*f* orbitals are treated as core levels show that the band gap already vanishes due to some Eu 5*d* states contributing to states near the Fermi level. Therefore, the metallic character of $EuGe_2$ may be attributed to the crossing of Eu 5*d* states below the Fermi level, but we still cannot discount significant 4*f* character at its Fermi surface. It would thus be highly desirable to experimentally determine the predominant character of the charge carriers at the Fermi level. Currently, experimental efforts are focused on the synthesis and careful structural characterization of the high-pressure modification $SrGe_2$ with the same structure.

Acknowledgments

Svilen Bobev and Eric D. Bauer gratefully acknowledge the Laboratory directed Research and Development program and the Institute for Complex Adaptive Matter (ICAM) for the financial support of this work through Postdoctoral Fellowships. The work at LANL is done under the sponsorship of the US Department of Energy.

References

[1] E. Zintl, Angew. Chem. 52 (1939) 1.
[2] S.M. Kauzlarich (Ed.), Chemistry, Structure and Bonding of Zintl Phases and Ions, VCH Publishers, New York, 1996 and the references therein.
[3] H. Schäfer, Ann. Rev. Mater. Sci. 15 (1985) 1 (and references therein).
[4] R. Nesper, Prog. Solid State Chem. 20 (1990) 1 (and references therein).
[5] H.-G.v. Schnering, Angew. Chem. Int. Ed. Engl. 20 (1981) 33.
[6] J.L. Sarrao, Physica B 318 (2002) 87.
[7] P.G. Pagliuso, J.L. Sarrao, J.D. Thompson, M.F. Hundley, M.S. Sercheli, R.R. Urbano, C. Rettori, Z. Fisk, S.B. Oseroff, Phys. Rev. B 63 (2001) 092406.
[8] J.M. Lawrence, G.H. Kwei, J.L. Sarrao, Z. Fisk, D. Mandrus, J.D. Thompson, Phys. Rev. B 54 (1996) 6011.
[9] O. Helleis, H. Kandler, E. Leicht, W. Quiring, E. Wölfel, Z. Anorg. Allg. Chem. 320 (1963) 86.
[10] A. Widera, H. Schäfer, Mater. Res. Bull. 15 (1980) 1850.
[11] B. Huang, J.D. Corbett, Z. Anorg. Allg. Chem. 624 (1998) 1787.
[12] B. Huang, J.D. Corbett, Inorg. Chem. 36 (1997) 3730.
[13] E.I. Gladyshevskii, Dopl. Akad. Nauk Ukr. RSR 2 (1964) 209.
[14] (a) A.C. Larson, R.B. Von Dreele, GSAS-General Structure Analysis System; LAUR 86-748, Los Alamos National Laboratory, Los Alamos, NM, 1986;
(b) L.B. McCusker, R.B. Von Dreele, D.E. Cox, D. Louër, P. Scardi, J. Appl. Crystallogr. 32 (1999) 36.
[15] P. Hohenberg, W. Kohn, Phys. Rev. B 136 (1964) 864.
[16] W. Kohn, L.J. Sham, Phys. Rev. A 140 (1965) 1133.
[17] R.G. Parr, W. Yang, Density-Functional Theory of Atoms and Molecules, International Series of Monographs on Chemistry, Vol. 16, Oxford University Press, New York, 1989.
[18] O.K. Andersen, Phys. Rev. B 12 (1975) 3060.
[19] O.K. Andersen, O. Jepsen, Phys. Rev. Lett. 53 (1984) 2571.
[20] U. von Barth, L. Hedin, J. Phys. C 5 (1972) 1629.
[21] P. Blaha, K. Schwarz, P. Sorantin, S.B. Trickey, Comput. Phys. Commun. 59 (1990) 399.
[22] P. Blaha, K. Schwarz, G.K.H. Madsen, D. Kvasnicka, J. Luitz, WIEN2k, an augmented plane wave + local orbitals program for calculating crystal properties, Vienna University of Technology, 2001.
[23] J.P. Perdew, S. Burke, M. Ernzerhof, Phys. Rev. B 45 (1996) 3865.
[24] A. Szytula, J. Leciejewicz (Eds.), Handbook of Crystal Structures and Magnetic Properties of Rare Earth Intermetallics, CRC Press, Boca Raton, FL, 1994.
[25] P. Villars, L.D. Calvert (Eds.), Pearson's Handbook of Crystallographic Data for Intermetallic Compounds, 2nd Edition, American Society for Metals, Materials Park, OH, 1991.
[26] A. Iandelli, A. Palenzona, Crystal chemistry of intermetallic compounds, in: K.A. Gschneidner, L. Eyring (Eds.), Handbook on the Physics and Chemistry of Rare Earths, Vol. 2, North-Holland, Amsterdam, 1979, p. 1.
[27] T.B. Massalski (Ed.), Binary Alloy Phase Diagrams, American Society for Metals, Materials Park, OH, 1990.
[28] F. Merlo, A. Palenzona, M. Pani, J. Alloys Compds. 348 (2003) 173.
[29] R. Pöttgen, A. Simon, Z. Anorg. Allg. Chem. 622 (1996) 779.
[30] A.G. Tharp, G.S. Smith, Q. Johnson, Acta Crystallogr. 20 (1966) 583.
[31] J. Evers, G. Oehlinger, A. Weiss, Angew. Chem. 89 (1977) 673.
[32] J. Evers, G. Oehlinger, A. Weiss, Z. Naturforsch. B 34 (1979) 524.
[33] M. Loewenhaupt, Z. Phys. 267 (1974) 219.
[34] R.-D. Hoffmann, R. Pöttgen, Z. Kristallogr. 216 (2001) 127.
[35] L. Pauling, The Nature of the Chemical Bond, 3rd Edition, Cornell University Press, Ithaca, NY, 1960.
[36] J.D. Corbett, Angew. Chem. Int. Ed. 39 (2000) 670.
[37] E.A. Leon-Escamilla, J.D. Corbett, Inorg. Chem. 40 (2001) 1226.
[38] R.D. Shannon, C.T. Prewitt, Acta Crystallogr. B 25 (1969) 925.
[39] J.S. Smart, Effective Field Theories of Magnetism, Saunders, Philadelphia, PA, 1966.
[40] N.W. Ashcroft, D.N. Mermin, Solid State Physics, Saunders College, Philadelphia, PA, 1976.
[41] P. Kurz, G. Bihlmayer, S. Blügel, J. Phys.: Condens. Matter 14 (2002) 6353.
[42] G.A. Landrum, R. Dronskowski, R. Niewa, F.J. DiSalvo, Chem. Eur. J. 5 (1999) 515.
[43] R. Dronskowski, P.E. Blöchl, J. Phys. Chem. 97 (1993) 8617.
[44] G.J. Miller, unpublished results.